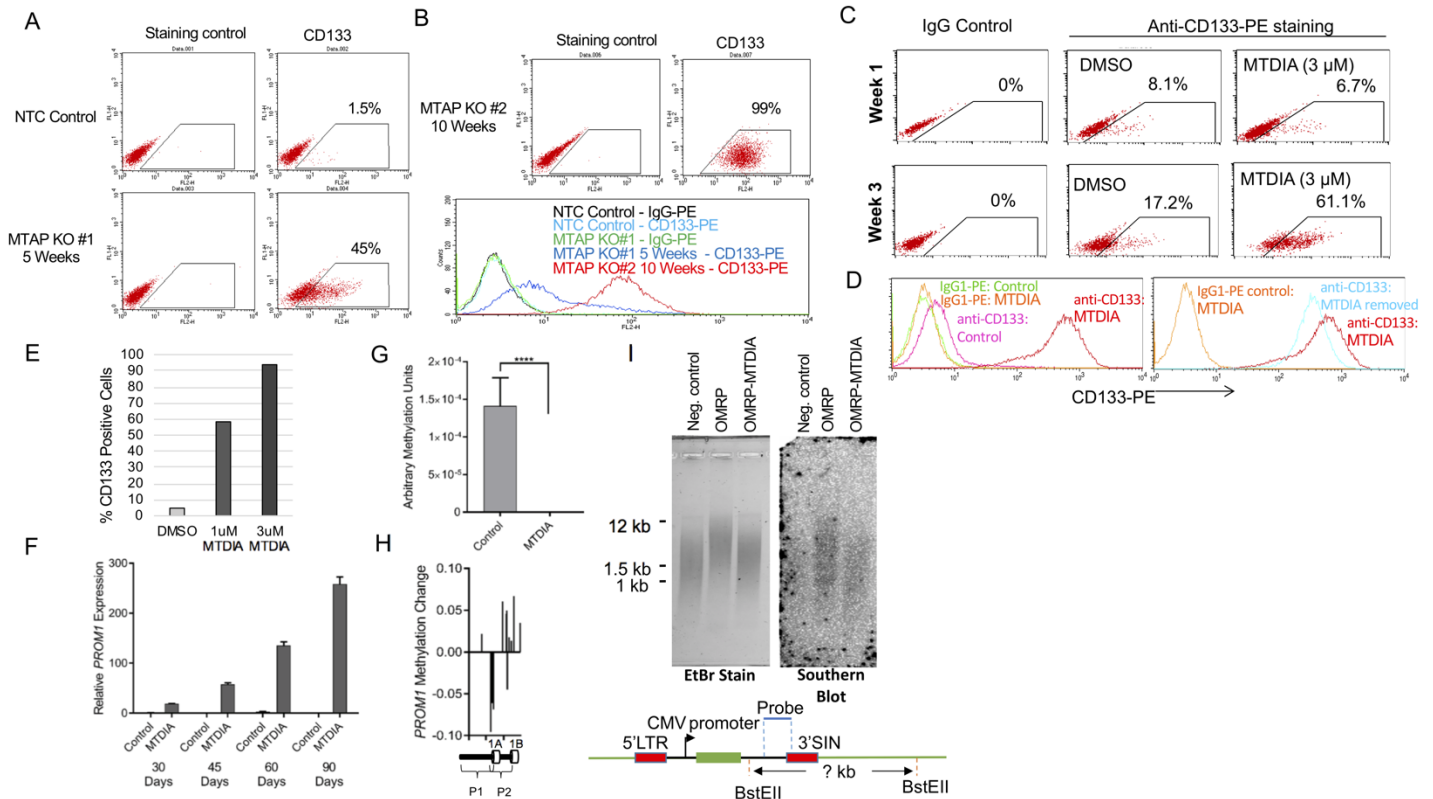


Supplementary Figure S1. MTAP loss results in MTA accumulation and increased tumorigenic potential in transformed astrocytes (A) Transduction of NHA cells with GFP (left) did not affect cell growth or morphology while transduction with OMRP transformation factors (right) resulted in a rapidly expanding population capable of spheroid growth. (B) Detection (by PCR) of successful *MTAP* gene knockout using primers that span the region of the *MTAP* locus targeted by CRISPR/CAS9 for excision. (C) Western blot confirmed loss of *MTAP* expression following CAS9-mediated gene knockout. (D) MTA measurement by LC-MS/MS confirms MTA accumulation following *MTAP* KO in transformed astrocytes. (E) Proliferation assay measuring transformed astrocytes under normal neural stem cell growth conditions, 2×10^5 cells plated per well, counted using a hemocytometer on day 3 and day 5. (F) MTA accumulation (measured by LC-MS/MS) in transformed astrocytes following *MTAP* inhibition with MTDIA. (G) Representative image showing increased sphere-formation (as opposed to aggregation) of MTDIA-treated cells compared with control. (H) Kaplan-Meier survival curves of nude mice that received intracranial transplantation of 10,000 transformed astrocytes that either were or were not subjected to MTDIA treatment during cell transformation (log-rank P value = 0.026). (I) Proliferation assay measuring transformed astrocytes under normal neural stem cell growth conditions, 2×10^5 cells plated per well, counted using a hemocytometer on day 3 and day 5. CRISPR, clustered regularly interspaced short palindromic repeats; GFP, green fluorescent protein; LC-MS/MS, liquid chromatography–tandem mass spectrometry; MTA, methylthioadenosine; *MTAP*, methylthioadenosine phosphorylase; MTDIA, methylthio-DADMe-Imunicillin; NHA, normal human astrocytes; NTC, non-targeting control;



Supplementary Figure S2. MTAP loss results in gradual upregulation of CD133/*PROM1* and altered methylation of the *PROM1* promoter in transformed astrocytes (A) Flow cytometry quantification of CD133-positive cells at 5-week time point shows significant upregulation of CD133+ cells in *MTAP* knockout cultures compared with the NTC. (B) Top: *MTAP* knockout in a separately transformed astrocyte culture shows homogeneously positive CD133-positive cells by 10 weeks post-transformation. Bottom: Histogram compares CD133 staining levels from control and *MTAP* knockout astrocyte cell lines. (C) Measurement of CD133 by flow cytometry after 1 and 3 weeks in control and MTDIA treated transformed astrocytes. (D) Histogram shows reversal of CD133 positivity after removing MTDIA from culture media. All cells were continuously maintained in stem cell media. (E) Summary of flow cytometry results showing dose dependent effect of MTDIA in upregulating CD133 expression. (F) *PROM1* expression measured by RT-PCR at varying time points after transformation shows progressive upregulation of *PROM1* expression with MTDIA treatment. (G) *PROM1* promoter methylation analysis using a methylation-sensitive qPCR method validates the methylation array results, showing decreased methylation after *MTAP* inhibition ($n=6$, t test P value $< 1 \times 10^{-4}$). (H) Methylation array probes from the *PROM1* promoter show relative decreased methylation (Parental/*MTAP* KO) following *MTAP* KO in transformed astrocytes. (I) Southern blot using DNA from normal blood (neg control), control, and MTDIA treated transformed astrocytes was performed to assess for monoclonal or oligoclonal selection. Schematic on bottom shows relative position of lentivirus components and the southern blot probe. EtBr, Ethidium Bromide; MTA, methylthioadenosine; *MTAP*, methylthioadenosine phosphorylase; MTDIA, methylthio-DADMe-Imunicillin A; *PROM1*, prominin-1; qPCR, quantitative polymerase chain reaction; RT-PCR, real-time PCR.

A Transformed Astrocytes, MTAP KO

Significantly Enriched Hypomethylated Pathways	Benjamini Hochberg p Value
Neuroactive ligand-receptor interaction	2.5E-2
Nicotine Addiction	2.2E-2
Wnt signaling pathway	2.6E-2
Morphine Addiction	3.3E-2
ECM-receptor Interaction	4.1E-2
Calcium Signaling Pathway	3.6E-2
Basal cell carcinoma	4.3E-2
Glutamatergic synapse	4.8E-2
Pathways in cancer	4.4E-2
Adrenergic signaling in cardiomyocytes	4.2E-2
Signaling pathways regulating pluripotency of stem cells	4.6E-2

Significantly Enriched Hypermethylated Pathways	Benjamini Hochberg p Value
Pathways in cancer	1.8E-4
Rap1 Signaling Pathway	2.7E-4
MAPK signaling pathway	2.8E-4
Ras signaling pathway	1.0E-3
Axon guidance	8.0E-3
Calcium signaling pathway	2.2E-2
Oxytocin signaling pathway	2.0E-2
Regulation of actin cytoskeleton	2.1E-2
Focal Adhesion	4.6E-2

B Transformed Astrocytes, MTDIA treated

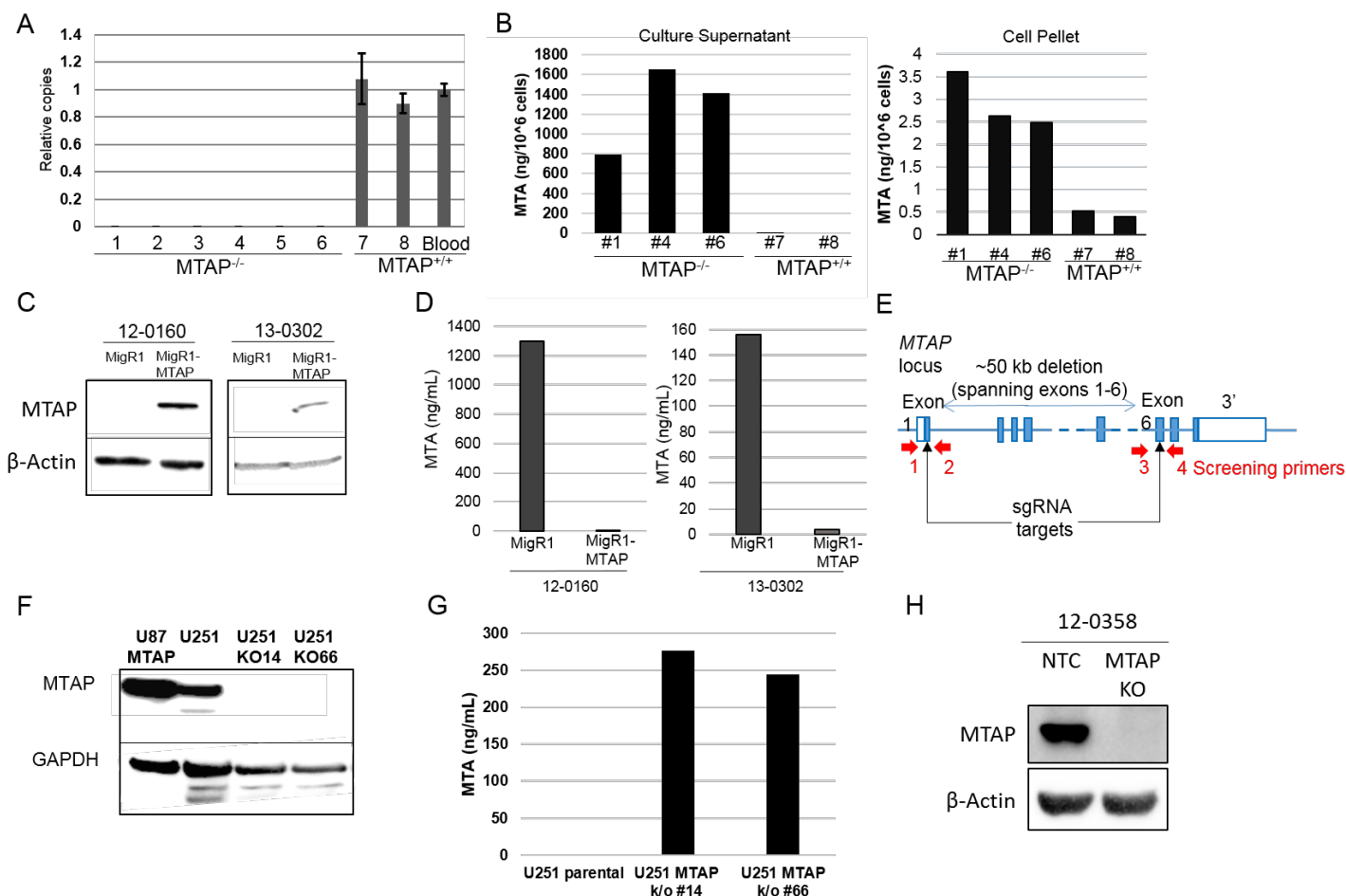
Significantly Enriched Hypomethylated Pathways	Benjamini Hochberg p Value
Pathways in cancer	1.2E-3
MAPK signaling pathway	1.7E-3
Signaling pathways regulating pluripotency of stem cells	1.4E-3
Rap1 Signaling Pathway	2.2E-2
Calcium Signaling Pathway	3.7E-2

Significantly Enriched Hypermethylated Pathways	Benjamini Hochberg p Value
Neuroactive ligand-receptor interaction	2.1E-4
MAPK Signaling Pathway	4.9E-3
Rap1 Signaling Pathway	1.1E-2
Ras Signaling Pathway	2.1E-2
Hypertrophic Cardiomyopathy	1.9E-2
Axon guidance	2.7E-2
cAMP Signaling pathway	2.6E-2
Arrhythmogenic right ventricular cardiomyopathy	2.9E-2

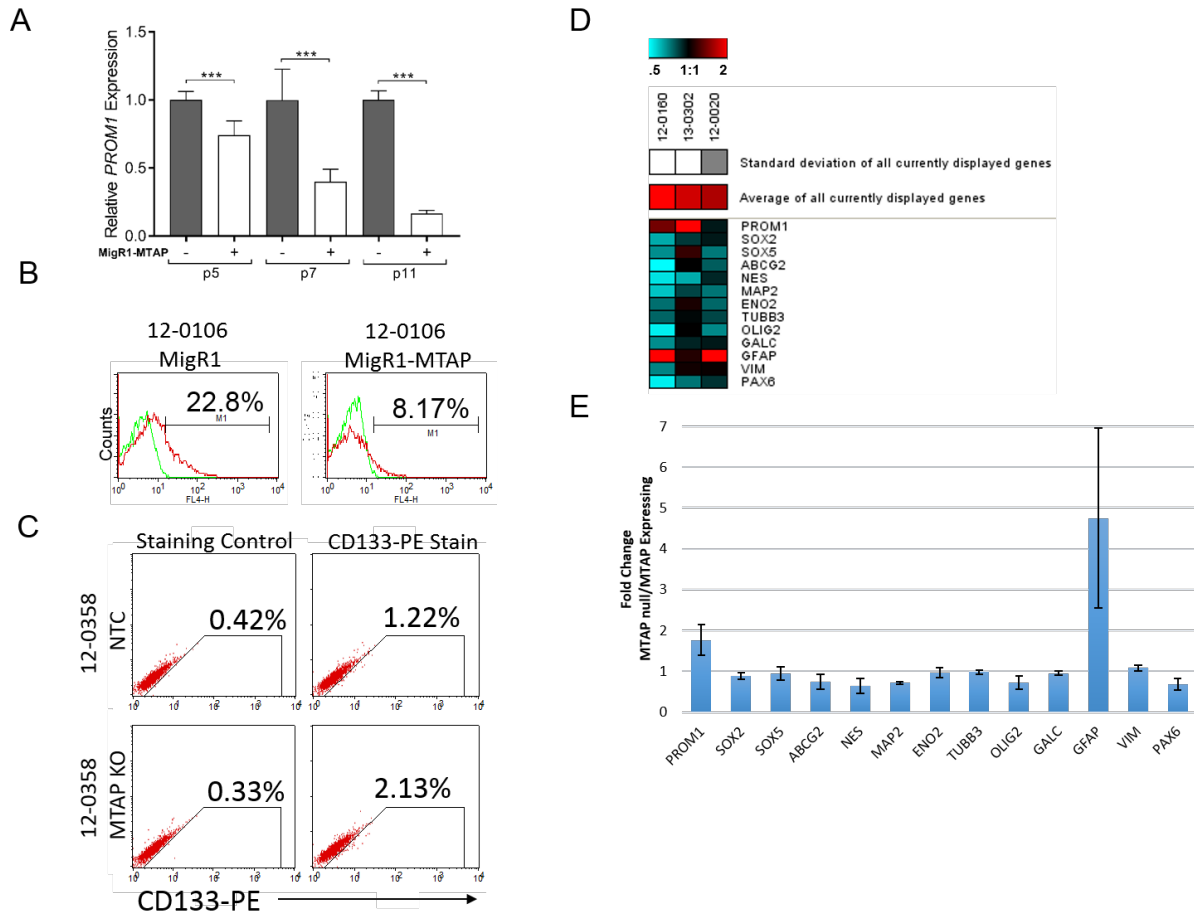
C

Data Set	Signaling Pathways regulating pluripotency of stem cells <u>Hypomethylated Gene CpG Islands</u>
Transformed Astrocyte, MTDIA treated	ACVR1C, AXIN1, BMP4, DLX5, DVL1, FGFR2, FGFR3, FGFR4, FZD1, FZD9, FZD10, HAND1, HNF1A, ID4, IGF1R, JAK3, LIF, MAPK11, MAP2K2, ONECUT1, OTX1, PAX6, PCGF3, PIK3R1, PIK3R3, SMAD5, TCF3, WNT3, WNT5A, WNT16, ZFHX3
Transformed Astrocyte MTAP KO	APC2, BMP4, DLX5, DVL1, DVL2, ESRRB, FGFR2, FZD10, HAND1, MAPK11, MEIS1, NEUROG1, ONECUT1, PAX6, PCGF6, PIK3CD, PIK3R1, WNT2B, WNT3, WNT7A, WNT7B, WNT9A, WNT11, WNT16, ZFHX3

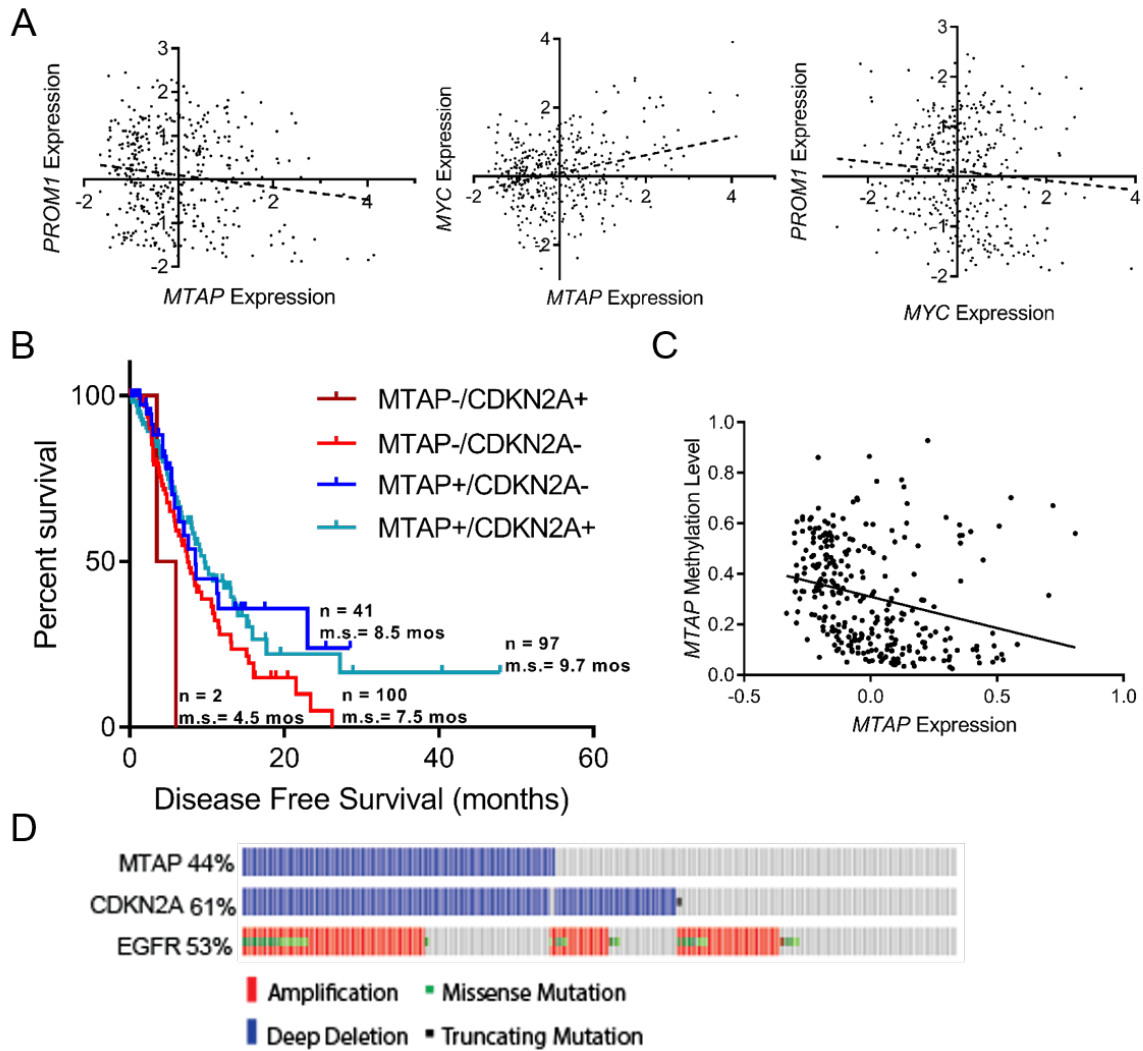
Supplementary Figure S3. Methylation analysis revealed pathways hypomethylated in MTAP-deficient or MTAP-inhibited cells. (A) Comparison of CpG island methylation loci in transformed astrocytes between parental cells and MTAP knockout cells shows altered methylation of displayed KEGG pathways. The top 3,000 genes (maximum allowed by DAVID platform) (>10% differential methylation) for each category were used as input to determine the enriched pathways. (B) The same analysis as in A except the comparison was made between DMSO control treated transformed astrocytes and astrocytes treated with MTAP inhibitor MTDIA. (C) Table showing specific gene promoter regions hypomethylated within the Kegg pathway Signaling Pathways regulating pluripotency of stem cells. DAVID, Database for Annotation, Visualization, and Integrated Discover; KEGG, Kyoto Encyclopedia of Genes and Genomes; *MTAP*, methylthioadenosine phosphorylase; MTDIA, methylthio-DADMe-Imunicillin A;



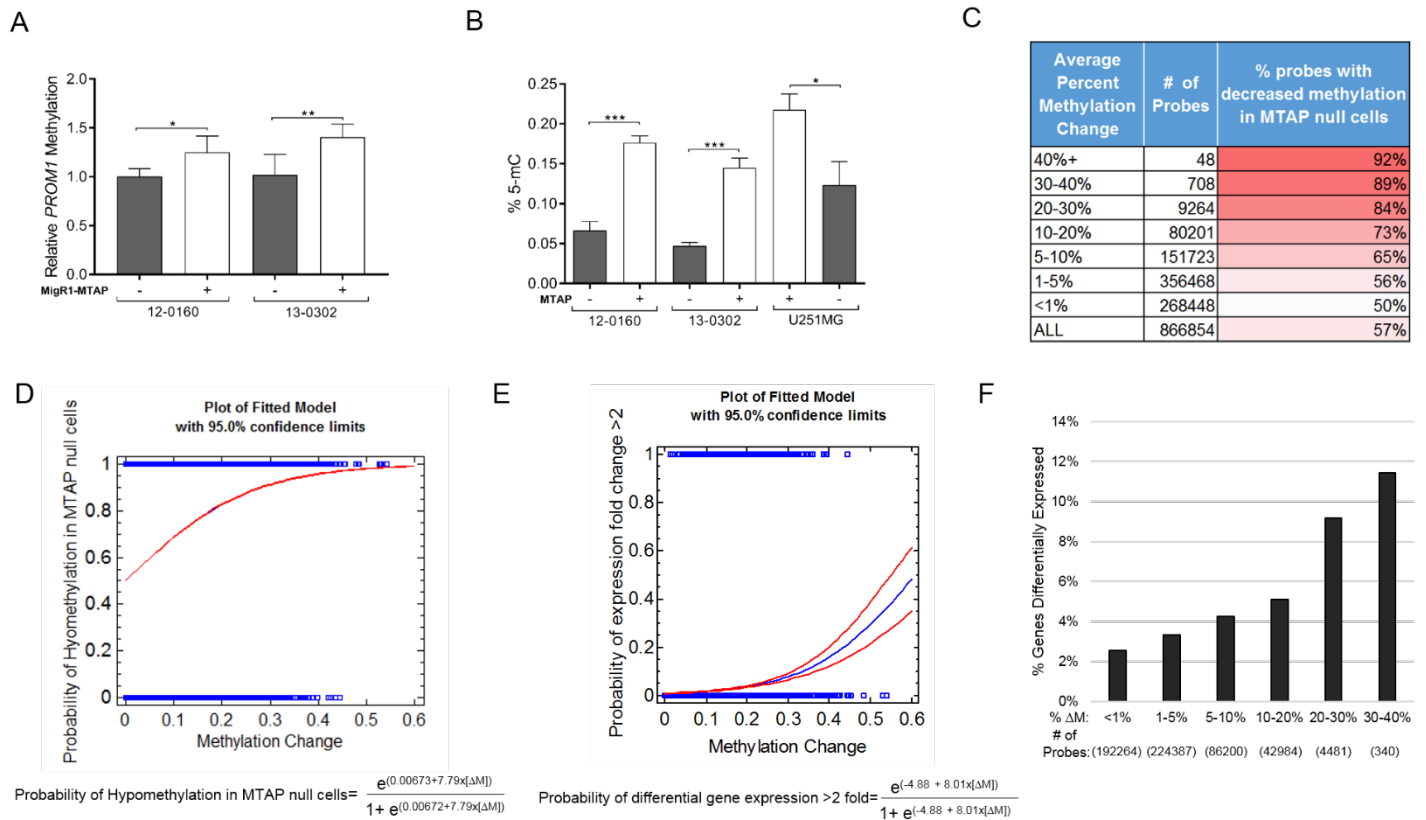
Supplementary Figure S4. Development of MTAP isogenic GBM experimental models. (A) Copy number real-time PCR was used to confirm *MTAP* status in 8 GBM tissue cultures (mean \pm SEM). (B) Measurement of MTA by LC-MS/MS shows dramatically elevated levels in culture media (left) and cell pellets (right) of *MTAP*-null cells. (C) Western blot showing *MTAP* restoration using MigR1 retroviral vector in *MTAP*-null cell lines and patient-derived cultures. (D) *MTAP* restoration in *MTAP*-null GBM lines results in dramatic reductions of MTA levels measured by LC-MS/MS. (E) Schematic showing strategy for CRISPR-mediated knockout of the *MTAP* gene in human U251MG cells. (F) Western blot showing loss of *MTAP* after CRISPR-CAS9-mediated gene knockout in two clones. Control lane (U87 *MTAP*) has *MTAP* overexpression. (G) MTA accumulation in U251MG cell culture media following *MTAP* knockout was confirmed by LC-MS/MS. (H) Western blot confirms *MTAP* knockout using CRISPR-CAS9 in 12-0358 *MTAP* WT patient-derived cell line. LC-MS/MS, liquid chromatography–tandem mass spectrometry; MTA, methylthioadenosine; *MTAP*, methylthioadenosine phosphorylase; PCR, polymerase chain reaction; SEM, standard error.



Supplementary Figure S5. MTAP deficiency is associated with elevated expression of *PROM1* and *GFAP* in patient-derived GBM cells under stem cell culture conditions (A) Measurement of *PROM1* expression by RT-PCR at different time points after MTAP restoration in 12-0160 cells shows progressive decrease of CD133 expression ($n \geq 6$, t test P value $*** < 5 \times 10^{-4}$, error bars = SEM). (B) Flow cytometry histograms show decreased CD133 signal after MTAP restoration in 12-0106 patient-derived GBM cells. Green lines represent IgG control staining. Red lines represent CD133 staining. Bar graph (bottom) quantifies the percent CD133+ cells from each cell line. (C) Flow cytometry was used to measure CD133 expression after MTAP knockout in 12-0358 MTAP WT patient-derived GBM cells. (D) Patient-derived GBM cells were cultured in stem cell media and gene expression microarray analysis was performed (See figure 2B), with a focus on differentiation markers (Same markers analyzed in patient samples, Fig. 4B). Fold change of differentiation markers was calculated for 3 isogenic pairs of patient-derived GBM cells. Fold difference is shown for MTAP null/MTAP expressing cells in each pair. (E) Average fold change (+/- SEM) across the three patient-derived cell pairs from (D) is shown for each differentiation marker. IgG, immunoglobulin G; *MTAP*, methylthioadenosine phosphorylase; *PROM1*, prominin-1; qPCR, quantitative polymerase chain reaction; RT-PCR, real-time PCR; SEM, standard error of the mean.



Supplementary Figure S6. TCGA data shows association of *MTAP* status with gene expression and survival. (A) *MTAP* expression is negatively correlated with *PROM1* expression (left; $R^2=.02$, $P < 5 \times 10^{-3}$) and positively correlated with *MYC* expression (middle; $R^2=0.08$, $P < 1 \times 10^{-4}$). *MYC* expression and *PROM1* expression have no significant correlation ($R^2=0.007$, $P = 0.09$). (B) Kaplan-Meier curves showing TCGA GBM patient survival from 281 patients with all 4 genotype combinations of *CDKN2A* and *MTAP*. (C) Comparison of *MTAP* gene expression and *MTAP* promoter DNA methylation (CpG 21801897) shows a negative correlation between methylation and gene expression levels ($R^2 = .07$, P value $< 1 \times 10^{-4}$), suggesting some *MTAP* intact samples may be epigenetically silenced. (D) Plot showing co-occurrence of *MTAP*, *CDKN2A*, and *EGFR* genetic alterations in 281 GBM patients from the 2013 TCGA GBM data set.



Supplementary Figure S7. MTAP loss is associated with hypomethylation, resulting in gene expression changes (A) Methylation-sensitive quantitative PCR shows increased methylation in the *PROM1* promoter following MTAP restoration (n=6, *t* test *P* value * < 0.05, ** < 0.005, error bars = SEM). (B) Global 5-mC ELISA (EpiGentek) shows DNA hypomethylation in MTAP-null cells compared to MTAP-expressing isogenic counterparts (*t* test *P* value * < 0.05, *** < 0.0005, error bars = SEM, n ≥ 6). (C) Table accounting for all probes in the illumina MethylationEpic DNA methylation array. Probes with greater methylation change between isogenic pairs are more likely to be hypomethylated in *MTAP* null cells. (D) Logistic regression provides a prediction for the probability of hypomethylation at any given locus in *MTAP* null cells based on the magnitude of methylation change seen at that locus between *MTAP*-null and *MTAP*-expressing cells (analysis of deviance *P* value < 1×10⁻⁴). (E) Logistic regression based on methylation and gene expression array data from GBM isogenic models (N=19500) shows increasing probability of gene expression fold change of greater than 2-fold with increasing change in methylation at any given locus (Analysis of deviance *P* value < 1×10⁻⁴) (F) Methylation probes (550,656) matched to 19,500 genes from the Affymetrix Human 2.0 Plus microarray show that increasing magnitude of methylation change (ΔM) at a given locus following *MTAP* restoration/knockout is associated with an increased likelihood of differential expression of the gene associated with that locus. Methylation change ΔM and expression fold change values in panels C-F were obtained by averaging the results from the 12-0160, 13-0302, and U251MG isogenic cell pairs. GBM, glioblastoma; *MTAP*, methylthioadenosine phosphorylase. ^a ΔM , increasing magnitude of methylation change.

A Combined 12-0160, 13-0302, U251MG

Enriched Hypomethylated Pathways	Benjamini Hochberg p Value
Signaling pathways regulating pluripotency of stem cells	4.9E-2
Enriched Hypermethylated Pathways	Benjamini Hochberg p Value
NA	NA

B TCGA GBM Samples

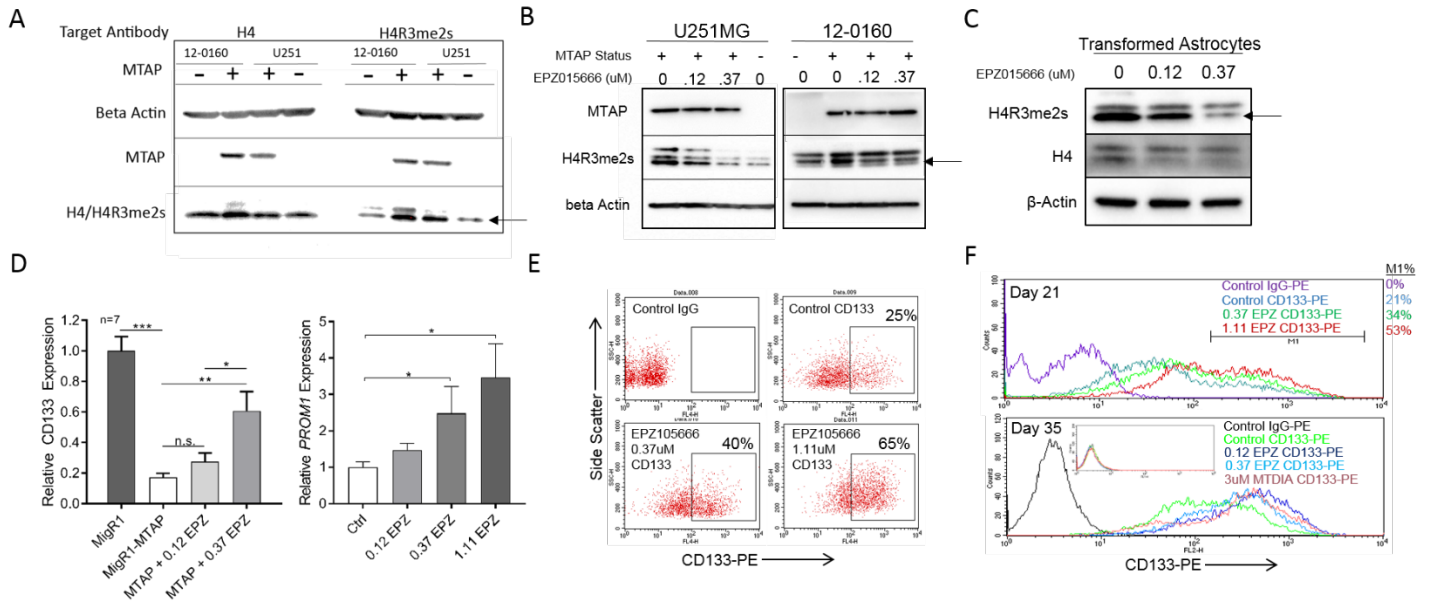
Significantly Enriched Hypomethylated Pathways	Benjamini Hochberg p Value
Neuroactive ligand-receptor interaction	8.9E-3
Transcriptional misregulation in cancer	1.0E-2
Maturity onset diabetes of the young	7.7E-3
HTLV-I Infection	8.9E-3
Nicotine Addiction	8.3E-3
Hippo Signaling Pathway	9.1E-3
Type II diabetes mellitus	8.1E-3
Retrograde endocannabinoid signaling	7.4E-3
Pathways in cancer	7.6E-3
Signaling pathways regulating pluripotency of stem cells	1.1E-2
Calcium Signaling Pathway	1.3E-2
MAPK signaling pathway	1.2E-2
Endocytosis	1.4E-2
Type I diabetes mellitus	2.0E-2
Cell adhesion molecules (CAMs)	2.2E-2
Focal Adhesion	3.7E-2
Synaptic Vesicle Cycle	4.3E-2
PI3K-Akt signaling pathway	4.9E-2

Significantly Enriched Hypermethylated Pathways	Benjamini Hochberg p Value
Pathways in cancer	1.2E-2
Cell adhesion molecules (CAMs)	2.1E-2
Neuroactive ligand-receptor interaction	4.3E-2
cAMP Signaling pathway	3.4E-2

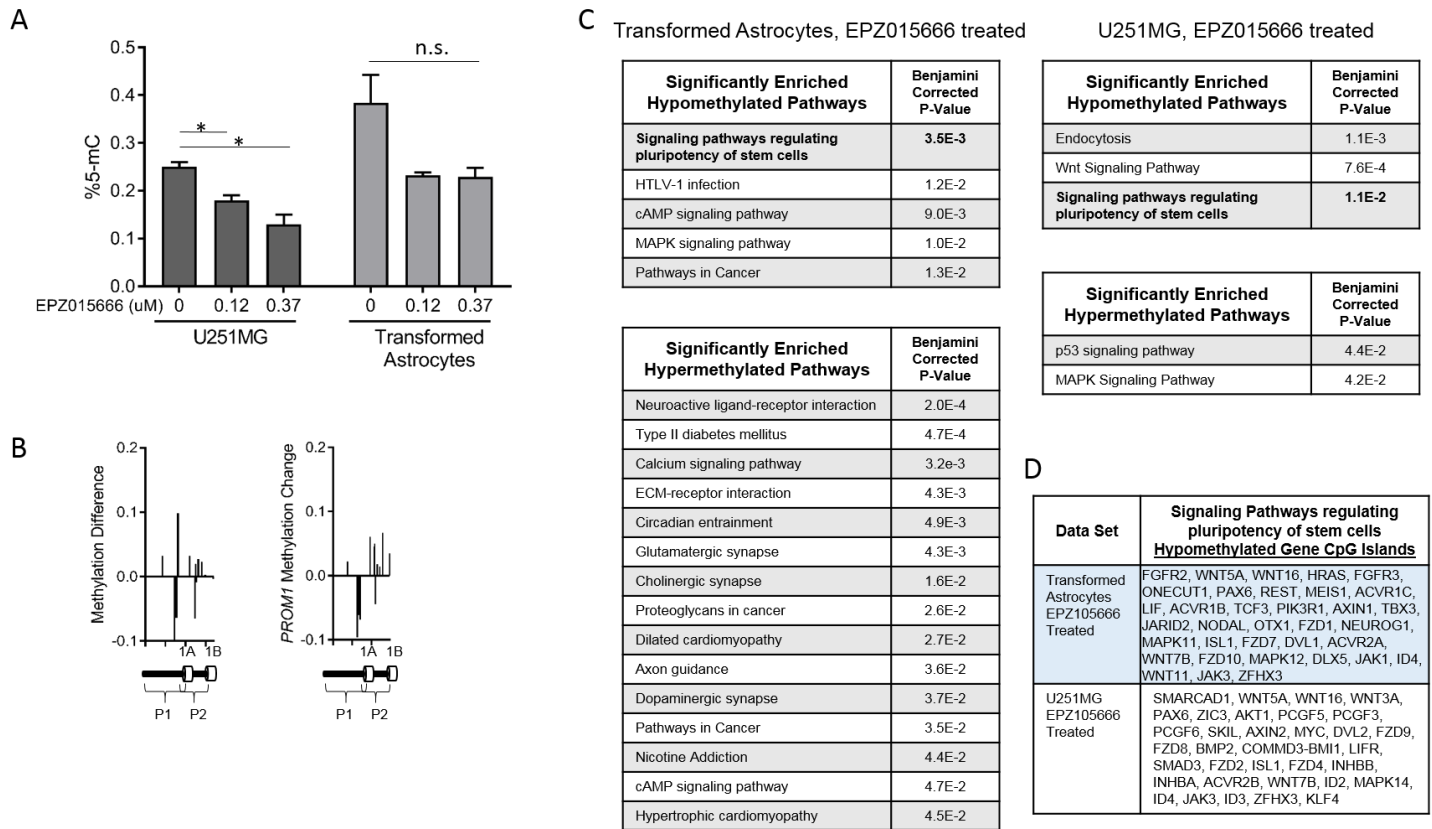
C

Data Set	Signaling Pathways regulating pluripotency of stem cells <u>Hypomethylated Gene CpG Islands</u>
GBM Cell MTAP null	BMI1, ESX1, FZD7, MAP2K2, NEUROG1, PIK3R5, REST, WNT7A
TCGA Low MTAP Expression	ACVR1C, DLX5, DUSP9, ESX1, FGFR2, FZD6, FZD8, FZD10, IGF1R, ISL1, JAK3, LHX5, NEUROG1, PAX6, PIK3R5, TBX3, WNT2B, WNT3A, WNT6, ZIC3

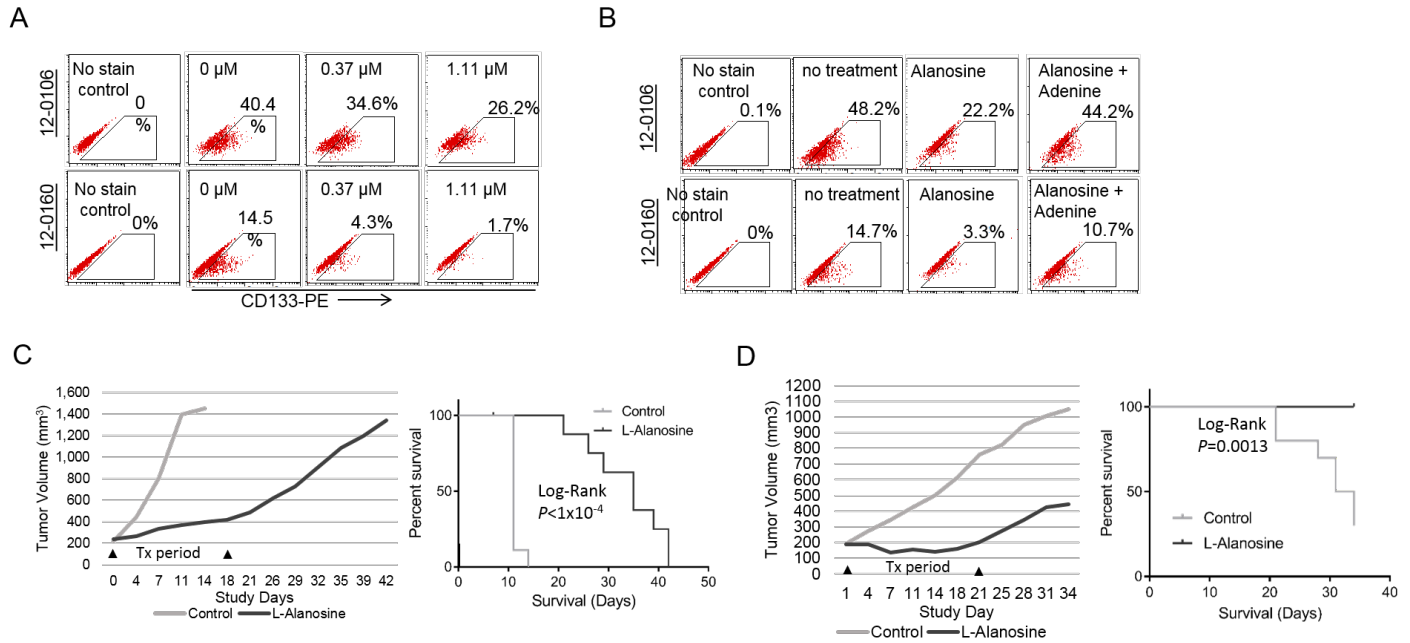
Supplementary Figure S8. Pathway analysis of hypomethylated gene promoters in MTAP-deficient cell lines and patient samples. (A) Comparison between *MTAP*-expressing and *MTAP*-null GBM cells was performed by calculating average beta value for each probe across 3 isogenic cell pairs, 12-0160, 13-0302, and U251MG. Probes were classified as either hypomethylated or hypermethylated in *MTAP*-null cells compared to *MTAP*-expressing cells and were analyzed using DAVID. Using the top 250 genes from each category (>20% methylation difference per probe) revealed only one significantly enriched pathway. No other set of input probes yielded any significantly enriched groups. (B) Analysis was performed as in (A) except methylation data from TCGA patient samples was grouped by *MTAP* expression into low- versus high-*MTAP*-expressing groups. Probes were classified as hypomethylated or hypermethylated in low-*MTAP*-expressing samples. Input of the top 3,000 genes for each category yielded the illustrated enriched pathways. (C) Individual hypomethylated genes in the KEGG pathway signaling pathways regulating pluripotency of stem cells from each sample set are shown. DAVID, Database for Annotation, Visualization, and Integrated Discover; KEGG, Kyoto Encyclopedia of Genes and Genomes; *MTAP*, methylthioadenosine phosphorylase; TCGA, The Cancer Genome Atlas.



Supplementary Figure S9. MTAP loss or PRMT5 inhibition by small molecule inhibitor EPZ015666 results in decreased H4R3me2s levels and upregulation of CD133. (A) Western blots showing MTAP restoration or *MTAP* knockout resulted in increased or decreased H4R3me2s levels, respectively. Arrow indicated H4R3me2s band. (B) Western blots showing H4R3me2s levels based on *MTAP* status and PRMT5 inhibition. (C) Western blot showing effect of PRMT5 inhibition on H4R3me2s levels in transformed astrocytes. (D) Left: Inhibition of PRMT5 with small molecule inhibitor EPZ015666 for 30 days rescues CD133 expression following *MTAP* restoration in 12-0160 *MTAP*-null GBM cells (data pooled from 2 experiments, *t* test *P* value * <0.05 , ** <0.005 , *** $<5 \times 10^{-4}$, n.s. = not significant, error bars = SEM). Right: *PROM1* expression in transformed astrocyte model following 14 days of EPZ015666 treatment (*t* test *P* value * <0.05 , error bars = SEM) (E) Flow cytometry shows impact of EPZ015666 treatment for 21 days on CD133 expression in transformed astrocytes. (F) Flow cytometry histogram of CD133 staining shows increased CD133 expression in EPZ015666- and MTDIA-treated samples compared with control. Inset shows non-staining controls. H4R3me2s, H4 arginine 3 dimethylation; PRMT5, Protein arginine methyltransferase 5; *MTAP*, Methylthioadenosine Phosphorylase; *PROM1*, Prominin1



Supplementary Figure S10. PRMT5 inhibition results in altered DNA methylation globally, affecting stem cell regulatory pathways. (A) 5-mC ELISA demonstrates decreased global methylation following EPZ015666 treatment for 30 days in *MTAP* wildtype U251MG cells and transformed astrocytes. **(B)** *PROM1* promoter methylation of transformed astrocytes is shown for control cells relative to EPZ015666-treated cells (Left panel), and to *MTAP* knockout cells for comparison (right panel). **(C)** Comparison of MethylationEPIC probes from gene CpG islands in cells cultured with or without PRMT5-inhibitor EPZ015666 shows significant enrichment of signaling pathway regulating pluripotency of stem cells, similar to what is seen after *MTAP* loss or inhibition (see Supplementary Figure S3). **(D)** Table showing genes hypomethylated following EPZ015666 treatment that are included in the KEGG Signaling pathways regulating the pluripotency of stem cells. KEGG, Kyoto Encyclopedia of Genes and Genomes.



Supplementary Figure S11. Purine deprivation by L-Alanosine treatment targets MTAP-null CD133-positive GBM cells. (A) Flow cytometry shows that L-Alanosine treatment for 3 days has a dose-dependent effect against CD133 positive cells in 12-0106 (top) or 12-0160 (bottom) cells. (B) Administration of exogenous adenine is able to rescue CD133-positive GBM cells from L-Alanosine toxicity. Cells were stained with anti-CD133 antibody and quantified by flow cytometry. (C) Left panel: Tumor growth of subcutaneous patient-derived GBM xenograft 10-0171 measured by handheld calipers shows growth suppression by L-Alanosine treatment ($n=8$ animals per arm). Right panel: Animal survival for subcutaneous 10-0171 xenografts shows prolonged survival with L-Alanosine treatment of animals in panel C (log-rank P -value $< 1 \times 10^{-4}$). (D) Left panel: Tumor growth of subcutaneous patient-derived GBM xenograft 12-0160 measured by handheld calipers shows growth suppression by L-Alanosine treatment ($n = 10$ animals per arm). Right panel: Animal survival for subcutaneous 12-0160 xenografts shows prolonged survival with L-Alanosine treatment (log-rank P -value = 0.0013).